ELSEVIER

Applied Catalysis A: General 205 (2001) 245–252

APPLIED CATALYSIS A: GENERAL

www.elsevier.com/locate/apcata

Characterisation by EPR and other techniques of $La_{1-x}Ce_xCoO_{3+\delta}$ perovskite-like catalysts for methane flameless combustion

Cesare Oliva [a,*], Lucio Forni [a], Andrea D'Ambrosio [a], Francesca Navarrini [a], Alexei D. Stepanov [b], Zakhar D. Kagramanov [b], Anatoli I. Mikhailichenko [b]

[a] *Dipartimento di Chimica Fisica ed Elettrochimica, Università degli Studi di Milano, CNR CSRSRC, via C. Golgi, 19 20133 Milano, Italy*
[b] *D.I. Mendeleev Chemical-Technological University of Russia, Moscow, Russia*

Received 19 January 2000; received in revised form 4 April 2000; accepted 5 April 2000

Abstract

Two differently prepared series of $La_{1-x}Ce_xCoO_3$ (x=0, 0.05, 0.1, 0.2), indicated by A and C, have been analysed by EPR at temperature ranging between 95 and 295 K, both before and after their use as catalysts for methane flameless combustion. At progressively lowering temperature, some samples showed a narrowing Lorentzian-shaped pattern. This has been attributed to the formation of ordered layer-like systems. A different behaviour has been noticed with the x=0.1 samples of both series. The formation of spin bags and of spin glass has been hypothesised with these samples. A correlation between EPR spectra and catalytic performance has been highlighted.

Keywords: Perovskites; Methane flameless combustion; EPR analysis

1. Introduction

Perovskitic samples of formula $La_{1-x}Ce_xCoO_3$ are well-known as quite active catalysts for exhaust gas depollution. Indeed, they have been successfully tested for CO oxidation with air [1] and NO reduction by CO [2]. The Co-based sites play a different role in these two reactions. Furthermore, only after the NO reaction with CO the samples showed a Lorentzian-shaped EPR line, linearly broadening with temperature [2]. This was attributed to spin–spin superexchange, occurring between nearest neighbour Co paramagnetic ions through O atoms. The temperature-dependent broadening was then attributed to spin–phonon interactions in layer-like crystals approximating two-dimensional antiferromagnets [2–20]. Such a structure is caused by oxygen-richer planes formed by Co–O–Co units, alternating with planes in which Co–□–Co structures prevail, □ indicating an oxygen vacancy. The stability of the Co–O–Co surface plane was found to reduce the catalytic activity of the sample for the oxidation of CO by NO, but simultaneously it decreased the crystal strains, favouring the catalyst durability.

Therefore, the observation of a single Lorentzian-shaped EPR line could suggest the formation of an ordered structure, generally connected to lower surface area and, therefore, to lower catalytic activity.

Aiming at better understanding this connection, in the present work we have examined some cobaltites as catalysts for methane flameless combustion. These samples have been analysed also by XRD and BET,

* Corresponding author. Fax: +39-02-70638129.
E-mail address: cesare.oliva@unimi.it (C. Oliva).

0926-860X/01/$ – see front matter
PII: S0926-860X(00)00572-X

looking for correlation between crystal structure, surface area, catalytic activity and EPR spectra.

2. Experimental

2.1. Materials

Two series of catalysts, referred to as A and C, have been prepared. The samples of the A series were obtained from oxide mixtures in molten ammonium nitrate, by calcination in air for 1 h at 1223 K, followed by grinding and further calcination at 1223 K for 32 h. The samples of the C series were obtained by calcination of their sol–gel citrate precursors up to 973 K for 2 h, then ground and recalcined in air at 1073 K for 5 h. BET surface area resulted ca. 0.7 and ca. 8 $m^2\,g^{-1}$ for A and C samples, respectively. Prior to use for methane oxidation, all catalysts have been activated for 1 h at 873 K in flowing air (20 $cm^3\,min^{-1}$).

2.2. Procedure

EPR spectra have been collected by means of a Bruker ESP300 spectrometer at temperature ranging between 95 and 295 K, before (N-labelled spectra) and after (U-labelled spectra) their use as catalysts for the methane flameless combustion.

A few U samples have been also examined after vacuum (3×10^{-3} Pa) treatment performed at room temperature for ca. 2 h and after a following 50 min oxygenation carried out in pure oxygen (1.4×10^{5} Pa) atmosphere.

At higher recording temperatures, the EPR spectra of any of the samples did not show any significant change and therefore, they are not here reported. The line-width of the Lorentzian-shaped lines have been obtained by fitting the experimental pattern by the Bruker SimFonia programme.

The catalytic activity was measured by loading 0.2 g of catalyst, diluted with 1.3 g of quartz powder of the same particle size (60–100 mesh) in a continuous tubular quartz microreactor, to which a mixture of 20 $cm^3\,min^{-1}$ of a 1 vol.% CH_4 in N_2+20 $cm^3\,min^{-1}$ of air was fed, while increasing temperature by 2 K min^{-1} up to 873 K.

Table 1
Trace impurities detected by XRD in the present perovskite-like catalysts

x value	Preparation method	Detected phases[a]
0	A	–
	C	Co_3O_4
0.05	A	CeO_2>La_2O_3
	C	–
0.10	A	La_2O_3>CeO_2
	C	La_2O_3>Co_3O_4
0.20	A	La_2O_3>Co_3O_4>CeO_2
	C	La_2O_3>Co_3O_4>CeO_2

[a] Overall amount <5%.

XRD patterns have been collected by means of a Philips PW1820 powder diffractometer, by employing the Ni-filtered Cu Kα radiation (λ=0.15148 nm). The solid phases have been recognised by comparison with literature data [21].

3. Results

3.1. XRD analysis

XRD analysis (Table 1) shows that at increasing values of the formula coefficient x increasing amounts of La_2O_3 segregates with both AN and CN samples. Furthermore, a small amount of CeO_2 phase forms with the former catalyst when x=0.05 and 0.1, whilst a minor amount of Co_3O_4 segregates with the latter catalyst when $x\geq0.1$.

3.2. EPR spectra

3.2.1. x=0, 0.05, 0.2 samples before use as catalysts ('N' samples)

The samples did not undergo any further treatment after preparation, or after catalytic use, and prior to spectra recording. At room temperature, asymmetric low-resolution EPR features were generally observed with both AN and CN samples (see, e.g. Fig. 1). Patterns of this kind did not change when the sample underwent room temperature high vacuum treatment, while after the following sample oxygenation this EPR pattern was partially substituted by a ca. 300 G single line centred at 3050 G. When lowering temperature the EPR spectrum did not change significantly

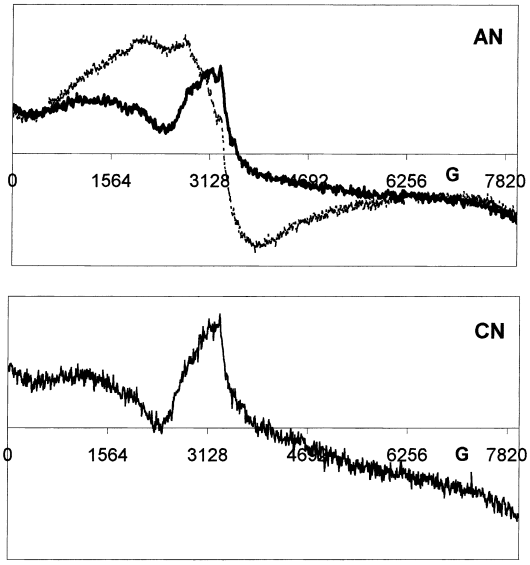

Fig. 1. Room temperature EPR spectra of AN and CN $LaCoO_{3+\delta}$ samples. (AN): dotted line 160 K, full line 298 K; (CN) 165 K (spectral profile independent of temperature).

with the x=0 CN sample (Fig. 1). By contrast, it became increasingly more symmetric with all the other samples. This spectral shape ended in a narrowing $g\cong 2$ Lorentzian-shaped line with the x=0.05 CN sample, as well as with the x=0.05 and 0.2 AN samples (Figs. 2 and 3) at low temperatures. The intercept and slope of the ΔH_{pp} versus T straight line, drawn by the usual least-squares method, were calculated as 909, 864, 424 G and 3.07, 4.87, 4.66 G K^{-1} for the x=0.05 AN and CN, and for the x=0.2 AN samples, respectively. (1 gauss (G)=10^{-4} T). No Lorentzian-shaped line was observed with the 0.2 CN sample, even at the lowest (100 K) temperature.

3.2.2. *x=0.1 samples before use as catalysts ('N' samples)*

Both AN and CN samples of this composition showed peculiar EPR spectra. Indeed, no spectral lines at all were observed in the usual $g\cong 2$ region at room temperature. By contrast, both these samples gave very intense EPR signals at a magnetic field value lower than 2000 G, broadening at lower temperatures. Furthermore, the EPR spectrum of the x=0.1 AN sample changed completely at ca. 100 K, becoming composed of two broad and intense lines,

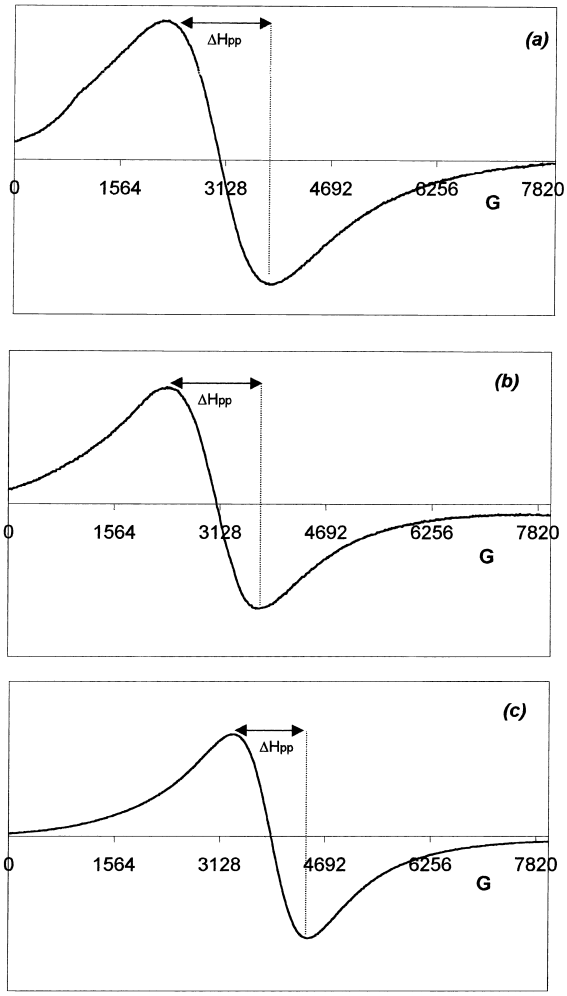

Fig. 2. Some Lorentzian-shaped EPR lines detected at 140 K. (a) x=0.05 CN; (b) x=0.05 AN and (c) x=0.2 AN. ΔH_{pp}=(a)1580 G; (b) 1360 G and (c) 1060 G (see also Fig. 3).

one of which centred at zero magnetic field value and characterised by a phase opposite to that of the symmetric line appearing at $g\cong 2$ (Fig. 4).

3.2.3. *x=0, 0.05, 0.2 samples after catalytic use ('U' samples)*

The samples showing a Lorentzian-shaped line when fresh generally retained such an EPR pattern after catalytic use (Fig. 5). Furthermore, also some samples characterised by an asymmetric EPR feature before catalytic use showed a Lorentzian-shaped line after reaction. This is the case of the x=0 and 0.2 CU

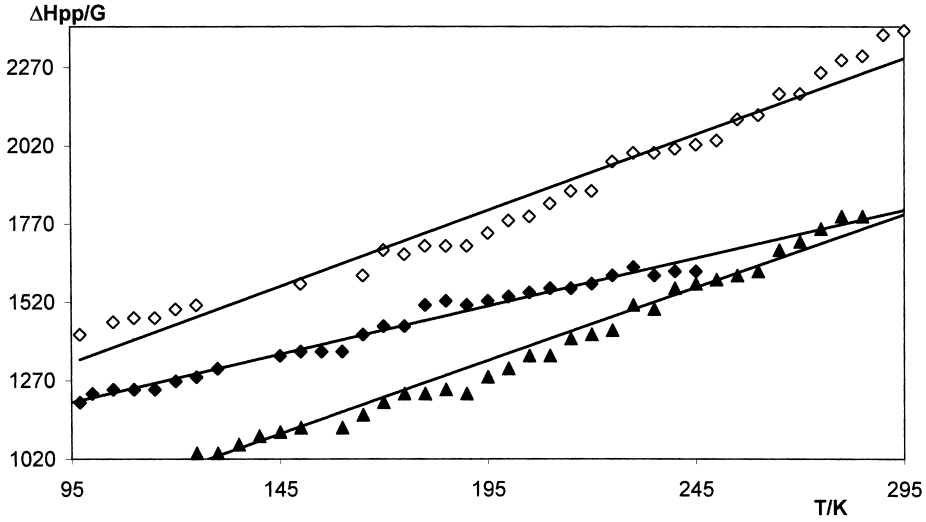

Fig. 3. Peak-to-peak width of the Lorentzian-shaped EPR line of $La_{1-x}Ce_xCoO_{3+\delta}$ samples. (◇) x=0.05 CN; (◆) x=0.05 AN and (▲) x=0.2 AN.

samples, which showed a single Lorentzian-shaped line narrowing from ca. 1465 to 1250 G (at T=100 and 295 K, respectively).

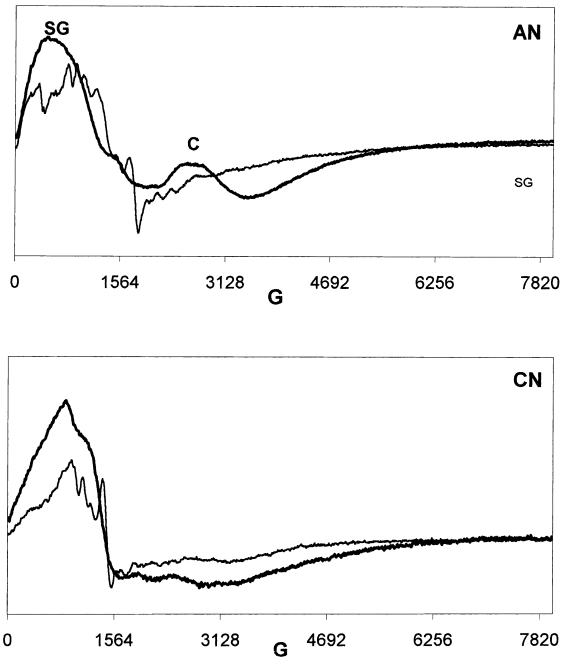

Fig. 4. Room temperature (more resolved, thinner track) and 100 K EPR spectra of $La_{0.9}Ce_{0.1}CoO_{3+\delta}$ of AN and CN series.

3.2.4. x=0.1 samples after catalytic use ('U' samples)

After catalytic use, the x=0.1 AU sample gave a temperature-independent Lorentzian-shaped EPR spectrum ($\Delta H_{pp} \cong 1400$ G). By contrast, the x=0.1 CU sample retained a broad asymmetric EPR feature at least down to ca. 100 K.

3.3. Catalytic activity

Our measurements showed that lower catalytic activity is obtained, as expected, with the lower-surface-area AN samples, with respect to the CN samples (Fig. 6). With the latter, for x>0.05 the conversion of methane increased a bit. By contrast, with the former the substitution of Ce for La depresses the catalytic activity at T>ca. 650 K. An atypical behaviour is shown by the x=0.1 AN sample, which is the worst catalyst at T<ca. 820 K, but the best one at higher temperatures. At lower reaction temperature, the x=0 CN sample was more active than the AN sample (Fig. 7). This difference was also retained when a small amount of Ce (x=0.05) substituted for La, because the catalytic activity of both samples decreased by the same ratio. However, when further amounts of Ce substituted for La, a different situation was observed at these temperatures with the two samples. Indeed, the activity

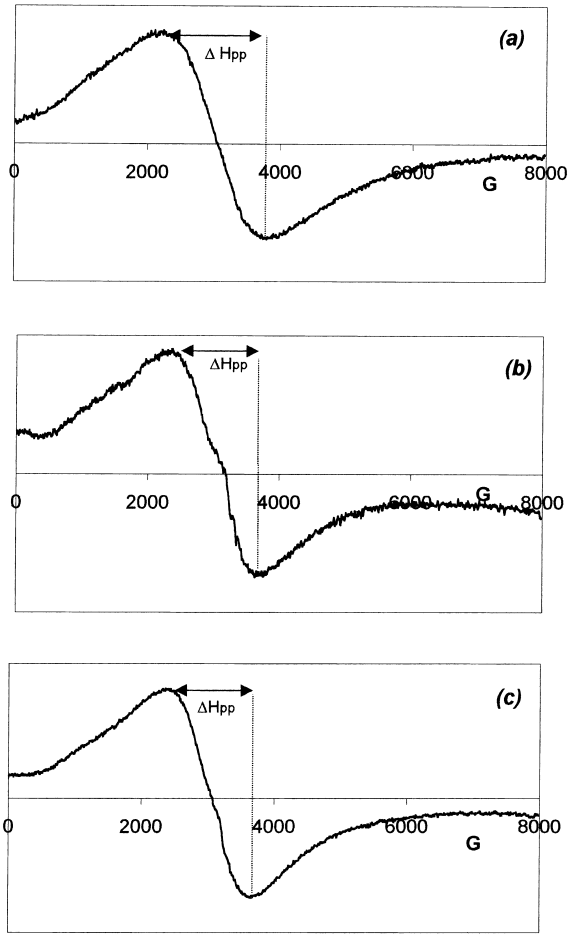

Fig. 5. Some Lorentzian-shaped EPR lines detected at 140 K. (a) x=0.05 CU; (b) x=0.05 AU and (c) x=0.2 AU. ΔH_{pp}=(a) 1570 G; (b) 1280 G and (c) 1280 G.

dropped to 0 with AN, while with CN samples it grew progressively.

4. Discussion

4.1. x=0; 0.05; 0.2 AN and CN samples

Generally [22] the $3d^6$ Co^{3+} ions are stable in the low spin ($S = 0, t_{2g}^6, e_g^0$) state when octahedrally coordinated to six oxygen atoms in an ideal $LaCoO_3$ structure. Ions of this kind can also form oxygen-based species such as Co^{3+}/O_2^- pairs [2,23,24]. However, in the present case, we cannot recognise these species

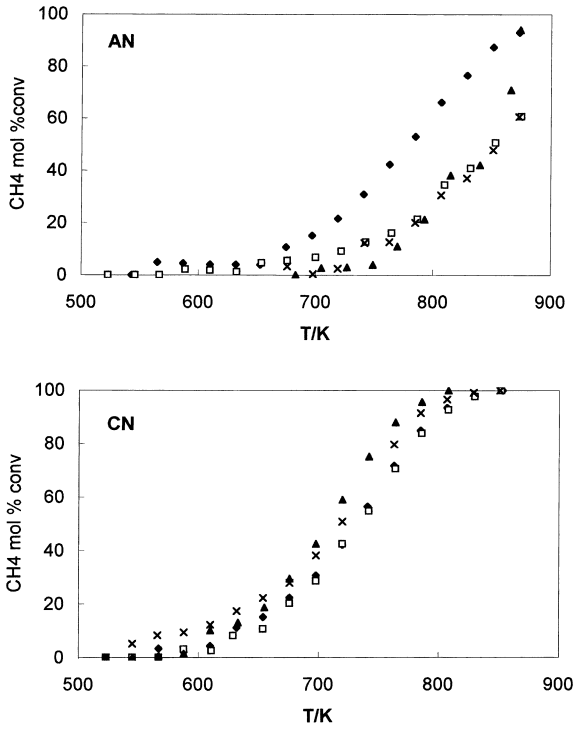

Fig. 6. Methane mol% conversion obtained with samples AN and CN (x=(◆) 0; (□) 0.05; (▲) 0.1; (X) 0.2).

in the very broad and low-resolution spectra detected at room temperature. These features are probably due to many different overlapping spectra. Therefore, in this paragraph the discussion will deal with well-fitted Lorentzian-shaped EPR lines only.

Oxidation of Co^{2+} to Co^{3+} in the catalyst is equivalent to creation of $h^\bullet$ electron holes, while the reduction back to Co^{2+} can be described as a reaction of $h^\bullet$ with an electron e^-. Therefore, the catalyst reoxidation process can be described [25] by the following reaction scheme:

$$O_{2,g} \leftrightarrow {O_{2,ads}}^- + h^\bullet \quad (1)$$

$${O_{2,ads}}^- \leftrightarrow {O_{2,ads}}^{2-} + h^\bullet \quad (2)$$

$${O_{2,ads}}^{2-} \leftrightarrow 2{O_{ads}}^- \quad (3)$$

$${O_{ads}}^- + {V_O}^{\bullet\bullet} \leftrightarrow O_O^x + h^\bullet \quad (4)$$

where ($^\bullet$) indicate the equivalence of introducing positive charges into the lattice. In Eq. (1), gaseous oxygen $O_{2(g)}$ reduces to ${O_{2,ads}}^-$, creating electron

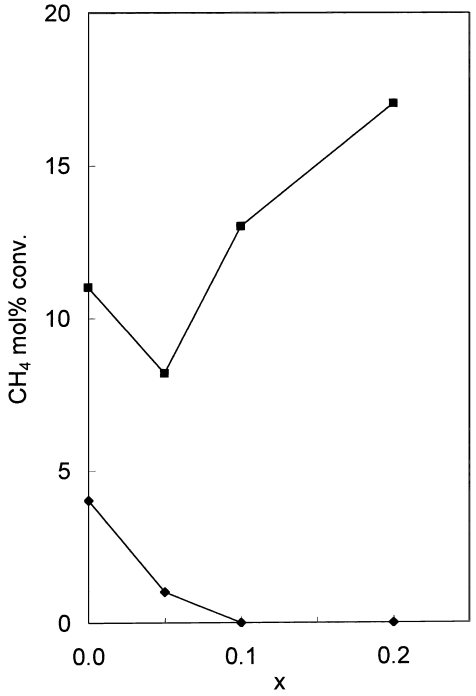

Fig. 7. Methane mol% conversion vs. x obtained at 630 K with samples AN (◆) and CN (■).

holes $h^{\bullet}$ (in particular, Co^{3+}). If the oxidation process stops, $O_{2,ads}{}^{-}$ can couple to Co^{3+} in $Co^{3+}/O_2{}^{-}$ pairs, as reported elsewhere [23,24]. On the other hand, $Co^{3+}/O_2{}^{-}$ can provide $O_{2(g)}$ to the suprafacial (low temperature) CH_4 oxidation, accompanied by Co^{3+} reduction to Co^{2+}. Intrafacial (high temperature) CH_4 oxidation would occur through extraction of the reticular oxygen O_o^x formed in Eq. (4). In any case, both these CH_4 oxidation processes would reduce the number of $h^{\bullet}$ electron holes, i.e. they would reduce some Co^{3+} to Co^{2+}. The presence of Co^{2+} ions would characterise also fresh catalysts when oxygen-deficient.

Co^{2+} can be either in the (S=1/2) low-spin state or in a (S=3/2) high-spin state. However, the latter is characterised by very fast relaxation times, giving [22] EPR spectrum at temperature lower than ∼20 K only. Therefore, only the (S=1/2) low-spin Co^{2+} ions are generally detectable. Indeed, we have found [2,26] that these ions, when octahedrally coordinated to oxygen, can form $–Co^{2+}–O^{2-}–Co^{2+}–O^{2-}$ chains. A Lorentzian-shaped single EPR line was observed in those cases and attributed to superexchange between Co^{2+} ions mediated by O^{2-}. The line-width of this feature was increasing with temperature and generally larger than 1000 G, as the EPR line here observed with fresh 0.05 AN, 0.2 AN, 0.05 CN catalysts (see Figs. 2 and 3) and with these (Fig. 5) and other samples after catalytic use. On the other hand, the deoxygenation–oxygenation experiments showed that the asymmetric EPR feature like that of Fig. 1 can be attributed to the catalysts in their reduced form, while adsorbed oxygen can be invoked to explain Lorentzian-shaped EPR lines. These are typical either of less active catalysts or of good catalysts but only after their use, i.e. when partially reoxidised. Indeed, these EPR lines are shown by the x=0.05 CN sample (Fig. 2(a)), which is the less active among the CN catalysts (Figs. 6 and 7), as well as by the x=0.05 and by the x=0.2 AN samples (Fig. 2(b) and (c)), which are the worst among the AN ones (see again Figs. 6 and 7). The x=0.1 AN sample will be discussed later.

Indeed, more ‘ordered’ structures, corresponding to lower surface areas and to less active catalysts, are also characterised by lower amounts of surface defects like $V_O^{\bullet\bullet}$ and therefore by a higher spin–spin exchange parameter J, as shown elsewhere [26] with other spinel-structured systems. This can explain the fact that the EPR Lorentzian-shaped lines are narrower with the x=0.05 AN sample than with the CN sample of the same composition (Figs. 2 and 3). At x=0 neither AN nor CN samples show the superexchange effect. This suggests that at x=0 more $V_O^{\bullet\bullet}$ are present in both these samples. A small amount (x=0.05) of Ce dissolved into their lattice is able in helping to fill these $V_O^{\bullet\bullet}$ vacancies by oxygen ions, restoring the $–O^{2-}–Co^{2+}–O^{2-}–Co^{2+}–$ system. Indeed, the substitution of Ce^{4+} for La^{3+} can be described by the reaction

$$Ce^{4+}O_2{}^{2-} \rightarrow Ce_{La}{}^{\bullet} + 2O_i{}^{2-} + h^{\bullet} + V_O^{\bullet\bullet} \qquad (5)$$

in which $Ce_{La}{}^{\bullet}$ is the defect due to the ionic substitution. The interstitial oxygen $O_i{}^{2-}$ can react with $V_O^{\bullet\bullet}$ forming reticular oxygen O_o^x, favouring a further intrafacial extraction. In any case, in Eq. (5) the number of $O_i{}^{2-}$ ions introduced into the lattice is two times the number of oxygen vacancies $V_O^{\bullet\bullet}$ created in it. Therefore, $O_i{}^{2-}$ can also fill $V_O^{\bullet\bullet}$ vacancies already present in the catalyst before the dissolution of cerium dioxide. Greater amounts of CeO_2 dissolve

into the AN samples lattice when x=0.2, completing the fulfilment of $V_O^{\bullet\bullet}$. Indeed, also with this sample a Lorentzian-shaped EPR line is observed, even narrower than with x=0.05 (Figs. 2 and 3). By contrast, the Lorentzian-shaped exchange-narrowed EPR line is no more observed with the x =0.2 CN sample. However, the XRD patterns show that a Co_3O_4 phase forms with this sample (Table 1), at difference with the analogous catalyst of the AN series. The presence of two Co-containing different phases in the x=0.2 CN sample can explain the loss of Co-based layer-like order and the consequent disappearance of the spin–spin superexchange phenomenon. Indeed, the Lorentzian-shaped EPR feature can be observed or not in Lanthanum cobaltites of the same nominal composition and surface area, depending also on the absence or presence of small amounts of extraneous phases.

For example, the fresh sample of nominal composition $La_{0.95}Ce_{0.05}CoO_3$ in our previous paper [2] did not show any Lorentzian-shaped EPR line though possessing a surface area ($6\,m^2\,g^{-1}$) even a bit smaller than that ($8\,m^2\,g^{-1}$) of the present C series sample. However, XRD analysis showed that greater amounts of segregated CeO_2 fcc phase were present in the former than in the latter sample (our unpublished results).

4.2. x=0.1 AN and CN samples

Up till now we have put on one side the x=0.1 AN and CN samples only. Indeed, their EPR spectra were completely different from those of the other catalysts, and so they have to be discussed separately. The fact that the EPR pattern at room temperature is composed by many overlapping features at magnetic field values lower than 2000 G (Fig. 4) can be explained on the base of the formation of ferromagnetic domains in these samples. Indeed, it is well-known [27–30] that among the O_{ads}^- species forming at Eq. (3) of the reoxidation process (vide supra) the magnetic attraction can overcome the electrostatic repulsion in the proximity of positive charges such as those brought about by cobalt ions. Therefore, if Eq. (4) does not occur, O_{ads}^- are allowed to group into spin bags within internal cavities, where they cannot react with adsorbed substrates. A similar explanation can be proposed for the room temperature spectra of Fig. 4. However, in this case the magnetic field at which the EPR patterns were observed was independent of temperature, at difference with other analogous literature cases [30] of spin bags formation. Therefore, we must hypothesise that the internal cavities of the x=0.1 AN and CN samples are saturated by O_{ads}^- spin bags even at room temperature, hindering them from growing up when cooling the sample.

The catalytic activity of these two samples has also a rather peculiar behaviour, being strongly decreasing with decreasing temperature. Furthermore, a temperature-dependent mechanism, able to reduce dramatically the catalytic activity at the lowest temperature (see Fig. 6 CN and Fig. 7), must be hypothesised with these samples. Indeed, as previously mentioned [31,32], the present catalytic reaction occurs through two mechanisms. The suprafacial one takes place at T<650 K, by involving the surface adsorbed oxygen only, while at higher temperature the reticular oxygen O_o^x moves faster to the surface through the intrafacial mechanism. The suprafacial catalytic activity of CN samples (Fig. 7) decreased when x=0.05, i.e. when a lower amount of $V_O^{\bullet\bullet}$ became available for oxygen adsorption. At higher x values, however, the suprafacial CN samples activity increased again, probably due to the previously mentioned partial segregation of La_2O_3, CeO_2 and Co_3O_4 phases. This does not occur with the x=0.1 AN samples (Fig. 7), in which CeO_2 segregates instead of Co_3O_4 (Table 1). In the last sample, therefore, Co paramagnetic (S=1/2) Co^{2+} ions, not organised in perovskitic $La_{0.9}Ce_{0.1}CoO_3$ nor in spinel Co_3O_4 phase, can be available to form spin glass [33] by interacting with each other and with the O_{ads}^- spin bags present in the sample. These new paramagnetic entities are observable at low temperature only, when they show a zero-field, phase-reversed broad band (Fig. 4, SG line). Indeed, this EPR feature is identical to that already observed by us [34] with a $La_{0.9}Sr_{0.1}CoO_3$ sample prepared by a different procedure. In that case, the formation of spin glass was demonstrated and the presence of spin glass decreased the catalytic activity, due to the link between cobalt ions and oxygen ions, and the consequent lower mobility of the latter. Similarly, the presence of spin glass in the x=0.1 AN sample at low temperature can explain its lower catalytic activity, with respect to the CN sample (Fig. 7). In the latter, the broad band at nearly zero magnetic field (Fig. 4) seems accompanied by other unresolved EPR overlapping features. Therefore, the formation of a

single spin glass phase cannot be safely affirmed in this case.

Furthermore, the spin glass creation is accompanied by the formation of ordered $–O^{2-}–Co^{2+}–O^{2-}–Co^{2+}–$ chains, as revealed by the $g \cong 2$ line (C in Fig. 4 AN) appearing at 100 K with the $x=0.1$ AN, but not with the $x=0.1$ CN catalyst. This fact is analogous to that reported with the mentioned Sr-containing catalyst [34] and further supports the observation that ordered structures always accompany a decrease of catalytic activity.

5. Conclusions

The Lorentzian-shaped EPR line observed at lower temperature can be attributed to superexchange occurring between Co^{2+} ions through O^{2-} ions in $–O^{2-}–Co^{2+}–O^{2-}–Co^{2+}–$ chains, typical of layer-like ordered crystalline structures. This spectroscopic feature is observed with Co-perovskite-like catalysts, depending also on their surface area and phase purity. Not all the samples here examined showed this spectroscopic feature. Indeed, the last seems typical of the catalysts less active for methane oxidation, or aged after their catalytic use. In any case, the presence of this Lorentzian-shaped line is always related to a loss of catalytic activity.

Acknowledgements

We are indebted with Italian Ministry of University and Scientific and Technological Research (MURST) for financial help allowing to provide a 6-months hospitality to two Russian students (A.D. Stepanov and Z.D. Kagramanov).

References

[1] L. Forni, C. Oliva, F.P. Vatti, M.A. Kandala, A.M. Ezerets, A.V. Vishniakov, Appl. Catal., B: Environ. 7 (1996) 269.
[2] L. Forni, C. Oliva, T. Barzetti, E. Selli, A.M. Ezerets, A.V. Vishniakov, Appl. Catal., B: Environ. 13 (1997) 35.
[3] T.G. Castner Jr., M.S. Seehra, Phys. Rev. B 4 (1971) 38.
[4] J.E. Drumheller, D.H. Dickey, R.P. Reklis, C.E. Zaspel, Phys. Rev. B 5 (1972) 4631.
[5] Z.G. Soos, K.T. McGregor, T.T.P. Cheung, A.J. Silverstein, Phys. Rev. B 16 (1977) 3036.
[6] R.D. Willet, R.J. Wong, J. Magn. Reson. 42 (1981) 446.
[7] M. Zomack, K. Baberschke, S.E. Barnes, Phys. Rev. B 27 (1983) 4135.
[8] G. Mozurkewich, J.H. Elliott, M. Hardiman, R. Orbach, Phys. Rev. B 29 (1984) 278.
[9] S.E. Barnes, Phys. Rev. B 30 (1984) 3944.
[10] D.L. Leslie-Pelecky, J.A. Cowen, Phys. Rev. B 48 (1993) 7158.
[11] D.L. Leslie-Pelecky, F. Vanwijland, C.N. Hoff, J.A. Cowen, J. Appl. Phys. 75 (1994) 6489.
[12] A. Shengelaya, G.-M. Zhao, H. Keller, K.A. Mueller, Phys. C (Amsterdam) 77 (1996) 5296.
[13] S.B. Oseroff, M. Torikachvili, J. Singley, S. Ali, S.-W. Cheong, S. Schultz, Phys. Rev. B 53 (1996) 6521.
[14] M.S. Seehra, M.M. Ibrahim, V.S. Babu, G. Srinivasan, J. Phys.: Condens. Matter 8 (1996) 11283.
[15] B.I. Kochelaev, R.G. Deminov, L.R. Tagirov, Phys. Solid State 38 (1996) 1263.
[16] C.E. Zaspel, J.E. Drumheller, Int. J. Modern Phys., B 10 (1996) 3649.
[17] S.E. Lofland, P. Kim, P. Dahiroc, S.M. Bhagat, S.D. Tyagi, S.G. Kara Bashev, D.A. Shulyatev, A.A. Arsenov, Y. Mukovskii, Phys. Lett. A 233 (1997) 476.
[18] D.L. Huber, J. Appl. Phys. 83 (1998) 6949.
[19] M. Tovar, M.T. Causa, G. Ibañez, C.A. Ramos, A. Butera, F. Rivadulla, B. Alascio, S.B. Oseroff, S.-W. Cheong, X. Obradors, S. Piñol, J. Appl. Phys. 83 (1998) 7201.
[20] C. Oliva, L. Forni, P. Pasqualin, A. D'Ambrosio, A.V. Vishniakov, Phys. Chem. Chem. Phys. 1 (1999) 355.
[21] Selected Powder Diffraction Data, Miner. DBM (1–40) JCPDS, Swarthmore, PA, 1974–1982.
[22] A. Abragam, B. Bleaney, Electron Paramagnetic Resonance of Transition Ions, Dover, New York, 1986 (Chapters 9 and 10).
[23] D. Cordischi, V. Indovina, M. Occhiuzzi, A. Arieti, J. Chem. Soc., Faraday Trans. 1 75 (1979) 533.
[24] E. Giamello, Z. Sojka, M. Che, A. Zecchina, J. Phys. Chem. 90 (1986) 6084.
[25] P.J. Gellings, H.J.M. Bouwmeester, Catal. Today 12 (1992) 1.
[26] C. Oliva, L. Forni, L. Formaro, Appl. Spectrosc. 50 (1996) 395.
[27] H. Thomann, R.A. Klemm, D.C. Johnston, P.J. Tindall, H. Jin, D.P. Goshorn, Phys. Rev. B 39 (1988) 6552.
[28] R.A. Klemm, H. Thomann, D.C. Johnston, Phys. Rev. B 37 (1988) 2239.
[29] K.C. Hass, in: H. Ehrenreich, T. Turnbull (Eds.), Solid State Physics, Vol. 32, Academic Press, New York, 1989, p. 237.
[30] C. Oliva, L. Forni, A.V. Vishniakov, Appl. Magn. Reson. 14 (1998) 283.
[31] T. Seiyama, in: L.G. Tejuca, J.L.G. Fierro (Eds.), Properties and Applications of Perovskite-type Oxides, Marcel Dekker, New York, 1993, p. 215.
[32] D. Ferri, L. Forni, Appl. Catal., B: Environ. 16 (1998) 119.
[33] M.D. Sastry, K.S. Ajayakumar, R.M. Kadam, G.M. Phatak, R.M. Iyer, Phys. C 60 (1988) 1330.
[34] C. Oliva, L. Forni, A.V. Vishniakov, Spectrochim. Acta A 56 (2000) 301.